Technical Annals

Vol 1, No 1 (2022)

Technical Annals

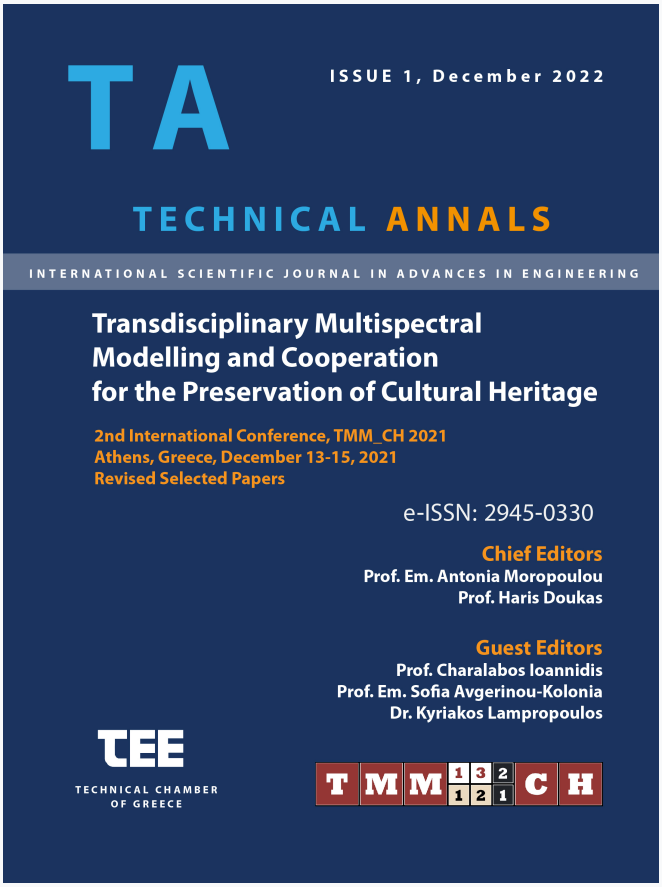

Inspecting the healing process in an artificial stone used for repair works containing crystallines

Evangelia Tsampali , Stamatios Amanatiadis , Georgios Karagiannis , Maria Stefanidou

doi: 10.12681/ta.32160

To cite this article:

Tsampali , E., Amanatiadis , S., Karagiannis , G., & Stefanidou , M. (2022). Inspecting the healing process in an artificial stone used for repair works containing crystallines. *Technical Annals*, *1*(1), 152–162. https://doi.org/10.12681/ta.32160

Inspecting the healing process in an artificial stone used for repair works containing crystallines

Evangelia Tsampali[1], Stamatios Amanatiadis[2], Georgios Karagiannis[2,3], Maria Stefanidou[1]

[1] Laboratory of Building Materials, School of Civil Engineering, Aristotle University of Thessaloniki, Greece
[2] Ormylia Foundation, Ormylia Art Diagnosis Centre, Greece
[3] Diagnosis Multisystems, N. Moudania, Chalkidiki, Greece
stefan@civil.auth.gr

Abstract. Stone has been a basic building material of different monuments and structural components such as foundations and masonry. At the same time, different types of stones have been used for decorative architectural elements, such as cornices, reliefs, colonnettes, and corbels. The maintenance of stone elements is essential for the continuity of these structures. Many studies have been performed to produce stones with artificial materials. This study aims to present a new approach to artificial stone with self-healing capability. Crystallines have been implied in two different dosages: 0.8 and 1.6% w./w, to achieve this goal. The addition of the crystalline admixtures affected the physical properties, decreasing the porosity and the capillary absorption, proving the sealing properties of the admixtures. The self-healing efficiency has been tested with the sorption test, recovery of compressive strength, and 3D acoustic microscopy. The crystalline admixtures accelerate the self-healing, increasing the sealing efficiency by 20% and recovering compressive strength by 15%. The analysis by 3D tomography provided results that confirm the healing of the crack hasn't occurred only on the surface but extended to a certain depth.

Keywords: Artificial stone, Healing, Mechanical Properties, Physical Properties, 3D acoustic tomography.

1 Introduction

Various types of stones have been employed in constructing monuments and historic buildings based on their significance and structural requirements as well as the availability of raw materials. Nowadays, many difficulties arise during restoration works when filling missing parts or replacing stone elements is required. These are

mainly attributed to the availability of specific stone types, the high cost of quarrying and transportation, and the high environmental impact. Artificial stone is an environmentally friendly alternate solution designed using guidelines and criteria based on the recorded properties of the authentic stones [1]. The term "artificial stone" has been specified in the Encyclopedic Dictionary of Polymers as [2]: "Special concretes and tiles, artificially colored to simulate natural stone, obtained by mixing stone dust aggregate and chips with Portland cement". The ability to produce a durable material of high-strength and resistance, which at the same time could be aesthetically elegant, imitating natural stones, is nowadays an extensive research field [3]. Today, the advantages of artificial stone compared to natural stone are very much in line with sustainability principles in construction, associated with reducing raw materials and the consumption of energy resources [4]. However, this research field is becoming even more interesting as the designed materials can heal their flaws. The concept of self-healing is directly related to the concept of resilience. Cracks generally increase the material's porosity and allow water, salts, and other harmful substances to enter the mass and damage the material. The leading causes of cracking are low resistance to tensile, thermal shrinkage, autogenous shrinkage, and drying shrinkage. Different design measures can restrict the shrinkage phenomena. Nevertheless, it seems that early cracking is unavoidable for materials exposed to the environment. The capacity of a material to heal the early formed cracks is a broad research topic and approached in different ways, one of which is crystallines in the mixture [5-6]. Crystallines, whatever their chemical composition, are hydrophilic substances. The presence of water is necessary to activate their action. If it is available, the crystalline admixtures (CA) react with it and cement to produce a new material that fills the cracks [7-8]. The use of artificial stone with healing capacities in heritage structures, poses several benefits, including the following options:

- Design a material of similar physical (porosity, texture, color hue, apparent specific gravity, etc.), mechanical properties, and microstructures with the original stone in the light of compatibility.
- Determine specific properties of the final product according to the specific needs of the monument and the broader environmental aspects (water retentivity, frost action, durability).
- Offer flexibility in the manufacture, application, and reproduction process.
- Cost-effectiveness and preservation of raw materials resources, under the prism of sustainability.
- Revival of a diachronic constructional technique that prevailed in constructions from the Neolithic period until the 20th century.
- Produce a material with self-healing capacities that increases its durability and reduces its preservation cost

The healing efficiency achieved in the materials tested is checked through different techniques such as strength recovery, sorption and porosity measurements. Additionally, a novel technique of acoustic microscopy that has been used in this study for the evaluation of healing is based on emitting and receiving high frequency (>10MHz) ultrasonic waves, i.e., shorttime pulses [9]. The received wave consists of the backscattered reflections, or echoes, of the emitted wave which results from the micro

structures on and under the surface of an object. The received signal consists of a few time-delayed pulses whose delay, or also called the time-of-flight, is associated with the distance the pulse traveled after it reflected from a microstructure. This signal is commonly called either the echograph or the amplitude scan (A-scan), while merging adjacent signals results in cross-sectional tomographic images, B-scans, or even planar representations of the inner structure, namely C-scans. It is worth mentioning that a proper excitation frequency must be selected since the trade-off between the resolution with the penetration depth should be considered.

The present study focuses on designing, manufacturing, and applying a series of tests on an artificial stone composition that imitates marble and can heal its weaknesses. The biggest challenge was to design an efficient artificial stone mixture for replacing or filling deteriorated marbles by maintaining the physic-mechanical properties of the authentic stones and enhancing their resilience under the current environmental-conditions. The artificial stone was created with inorganic binders such as white cement and natural pozzolan, natural aggregates of different gradations, and additives.

2 Experimental program and methodology

2.1 Experimental program

In this work, the effect of CAs has been investigated. The analysis was divided into two stages. In the initial stage, all compositions have been evaluated through compressive and flexural strength, porosity and capillary absorption. The second stage was estimating the healing efficiency, the crack closure, and the recovery of compressive strength. Additionally, a 3D acoustic tomography test has been depicted the depth of the healed crack.

2.2 Materials

In this study, Natural Pozzolan and Portland CEMI52.5 were used, classified by the EN 206-1:2000. The water to binder ratio was kept constant (0.45). The reference composition has further been modified by adding two different dosages equal to 0.8 and 1.6% w./w. of the binder. These percentages were chosen to test the limits and effectiveness of additives applied to concrete, as the manufacturer's proposal is somewhere between the two. Table 1 shows the mix designs of the investigated compositions. It is worth mention that the CA were added to the mixture without changing the other quantities.

Table 1. Mix designs of the investigated concretes.

Compositions	M	M0.8Cr	M1.6Cr
CEMI52.5	0.6	0.6	0.6
Natural Pozzolan	0.4	0.4	0.4
w/b	0.45	0.45	0.45
Limestone sand (0-4 mm)	1.5	1.5	1.5
Limestone aggregate (4-8 mm)	0.5	0.5	0.5
Crystallines **(CA)** (% w./w.)*	-	0.8	1.6
Superplasticizer (% w./w.)*	0.2	0.2	0.2
PP Fibers (% v./v.)	0.5	0.5	0.5
Consistence of fresh mortar (cm)	**14.5**	**15.5**	**15**

*the weight of the binder.

The superplasticizer addition (Rheobuild600) was added to maintain workability to the same level. Workability was measured for all compositions according to slump tests EN1015-3. Beam specimens, 40×40×160 mm^3, and cubic specimens 50×50×50 mm^3 were prepared. Compressive and flexural strength, porosity, capillary absorption, and ultrasonic pulse velocity were tested at 7, 28, and 90 days, according to EN196-1:1995, RILEM CPC 11.3, BA EN1015-15:2002 and EN12504-4:2004, respectively.

2.3 Evaluation of self-healing

The capillary water absorption (sorption) has been tested according to EN 13057:2002 standard but with pre-cracked specimens. Water absorption tests were performed after 7, 14, and 28 days of healing. The parameters for the water absorption test remain the same as the standard. The healing effect was estimated by calculating the Sealing Ration parameter as follows, Eq. (1):

$$SE = \frac{SC_{unhealed} - SC_{healed_{(\Delta t)}}}{SC_{unhealed} - SC_{uncracked}} * 100, \quad (1)$$

where: SE = Sealing Efficiency
$SC_{unhealed}$ = Sorption Coefficient for unhealed specimen ($g/cm^2/t^{1/2}$)
$SC_{healed\ (\Delta t)}$ = Sorption Coefficient after t days of healing ($g/cm^2/t^{1/2}$)
$SC_{uncracked}$ = Sorption Coefficient for the uncracked specimen ($g/cm^2/t^{1/2}$)

Similarly to the healing ratio, a crack closure ratio parameter was calculated based on equation (2):

$$Crack\_closure = \frac{CW_{initial_{(t_0)}} - CW_{healed_{(\Delta t)}}}{CW_{initial_{(t_0)}}} * 100, \quad (2)$$

where: $CW_{initial\ (t0)}$ = Crack Width after pre-crack.
$CW_{healed\ (\Delta t)}$ = Crack width after t days of healing.

Also, cubic specimens (50×50×50 mm^3) were pre-damaged at 28 days up to failure. Then the samples were cured for one month, immersed to tap water, and re-tested until failure again. The recovery of compressive strength (RCS), as a parameter, is set as follows, Eq. (3):

$$RCS = \frac{P_{healed\,(t=30days)}}{P_{undamaged\,(t=0)}} * 100, \quad (3)$$

where: $P_{healed\,(t=30\ days)}$ = Compressive strength of healed material after 30 days of healing (MPa)
$P_{undamaged(t=0)}$ = Compressive strength of undamaged specimen before the pre-damage (MPa)

Also, for this study a 3D acoustic tomography has analyze the healing depth, short wavelength pulses are utilized. In particular, a 75 MHz ultrasonic transducer is utilized to satisfy a fine spatial and vertical resolution (micrometric order), allowing a millimetric order penetration depth. Moreover, a powerful A/D converter is attached, namely 1 GSample/s, to enable the accurate surface characterization of the cracking

3 Results

3.1 Physic-mechanical properties

The physic-mechanical properties of all the compositions were tested at 7, 28, and 90 days of curing. The specimens were cured in a humid chamber with 99% HR and 25±2°C.

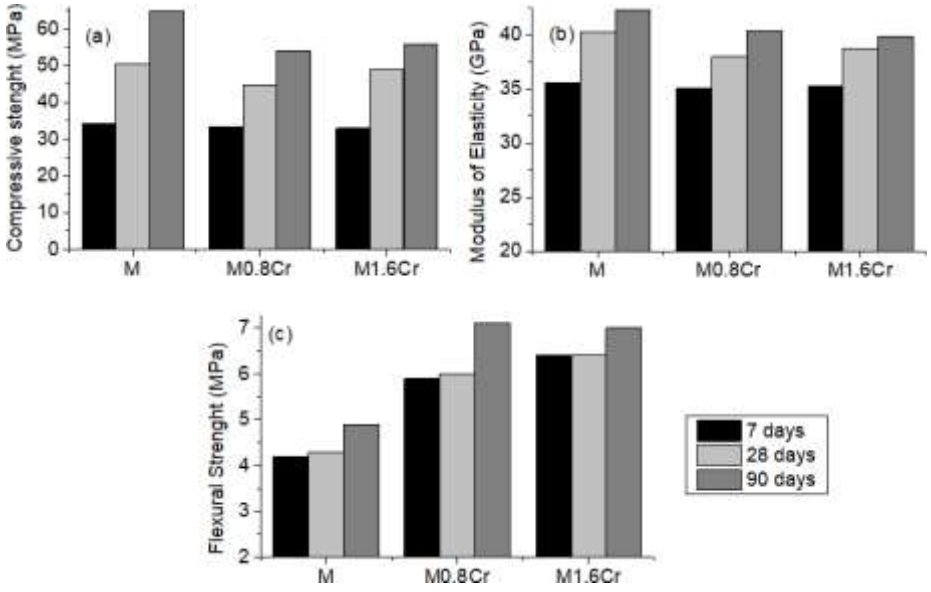

Fig. 1. Mechanical properties of the compositions, (a) compressive strength, (b) modulus of elasticity, (c) flexural strength after 7, 28, and 90 days of curing.

In figure 1(a), the compressive strength (CS) of all the compositions revealed that the addition of CAs seems to reduce it, especially after 90 days of hydration. Specifically, the addition of CA shows a reduction of CS at all ages. The CS of M0.8Cr composition compared to the reference sample decreased by 2.4%, 11.5%, and 16.7% at 7, 28, and 90 days. Additionally, the reduction of M1.6Cr was 3.8%, 3.1%, and

14.2% at 7, 28, and 90 days. Even though the reduction seems sugnificant, the final strength values meet the design criteria. According to figure 1(b), the modulus of elasticity seems to follow the same rate with the compressive strength, although the final reduction was 5.0% for the M0.8Cr, and 6% for the M1.6Cr.

In terms of flexural strength (FS), the CA seems to work favourably by increasing it (Fig. 1(c)). Specifically, the FS of M0.8Cr composition compared to the reference sample increased by 41.3%, 40.4%, and 44% at 7, 28, and 90 days, respectively. Furthermore, the increase of M1.6Cr was 51.4%, 47,7%, and 41.4% at 7, 28, and 90 days, respectively. These results show that CA eliminated the weak points by filling them and limited the discontinuities that can cause fracture due to tension.

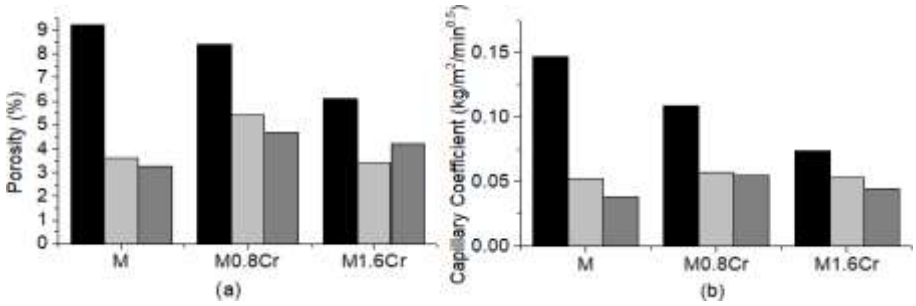

Fig. 2. Physical properties of the compositions, (a) porosity, (b) capillary coefficient after 7, 28, and 90 days of hydration.

The porosity test, time-related (Figure 2(a)), showed higher porosity at 7 days for the reference composition, indicating the crystalline effects at an early age. Although the M0.8Cr and M1.6Cr compositions' porosity at 90 days, compared to the reference, increased 43% and 28%, respectively. The same behavior was observed in figure 2(b) from the capillary coefficient, presenting a much lower absorption at seven days. Then, the reduction rate was lower than the reference sample. This reduction was may due to the hydrophilic nature of the crystallines.

3.2 Sorption coefficient test

The results of the water absorption test described in Section 2.3 are shown in Figures 3, and 4. Figure 3 depicts the relation of the level of damage of the cracked specimens, the initial crack measured with Dino-Lite microscope, and the initial slope of the water absorption. The level of damage has been measured with ultrasonic pulse velocity method, according to EN 12504-4:2004, before and after the pre-crack. The graph shows that the initial crack, although it was in the same range for all samples from 122 to 145 μm, does not play a primary role in the final absorption value.

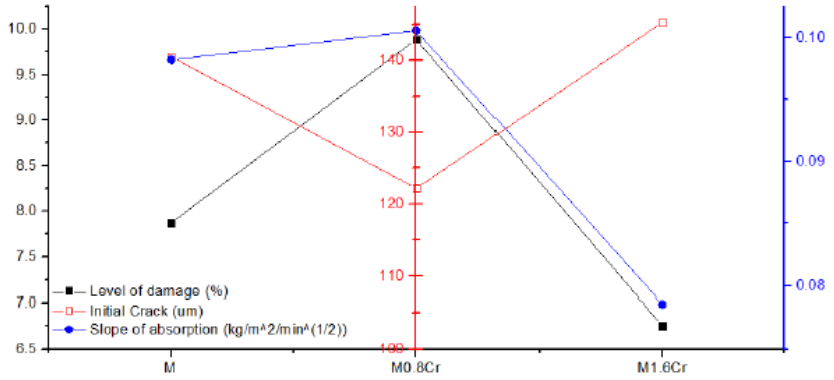

Fig. 3. Correlation between the level of damage, the initial crack, and the slope of absorption.

However, it is observed that the level of damage has a greater correlation with the final absorption. This fact showed that even the crack has been isolated for the sorption test, the sample's microstructure still plays a crucial role. Consequently, the initial and after healing slope can be used to evaluate the connectivity of the pore network. Figure 4 illustrates the difference in slope of absorption between the cracked and uncracked specimens. The porous media absorbs the water rapidly initially, and then the rate of absorption slows down. The water absorption rate of the cracked specimens increased, compared to the uncracked samples, due to the capillary tubes of the crack surface. In the reference sample, the slope of absorption of the uncracked and cracked specimens was 0.0334 kg/m^2/min$^{1/2}$ and 0.0982 kg/m^2/min$^{1/2}$, respectively. The slope of absorption of the uncracked specimens increased by approximately 194%. The slope of absorption of M0.8Cr was 0.0460 kg/m^2/min$^{1/2}$ and 0.1005 kg/m^2/min$^{1/2}$ for uncracked and cracked specimens, respectively, and the slope of water absorption of cracked specimens was 119%. Additionally, the slope of water absorption of the M1.6Cr cracked specimens fails to 76%, compared to the uncracked. The use of CA has increased the water absorption of the uncracked specimens due to the admixtures' hydrophilic nature and presented pretty similar results. Although in the case of the cracked specimens, the initial water absorption of the composition with 1.6% CA seems to decrease the capillary absorption already, even though the crack is wider.

The self-healing of cracked surfaces through further hydration of cementitious materials has two stages. The initial stage is the 'surface control' stage, in which unhydrated particles at the entrance of the crack react fast with the passing through water. Cause precipitation of hydrates on the surface, though further hydration. This mechanism plays a vital role in autogenous healing and provides most of the healing agents. The secondary-later stage is the 'diffusion control' stage. The ions inside the cement matrix diffuse and move to the cracked surface through capillary pores, generating additional self-healing products. Ca^{2+} ions with high concentrations exist in the capillary pores and in the cement matrix. When a crack occurs, the concentration difference between the crack and the inside of the matrix causes the Ca^{2+} ions to move to

the crack. When the Ca^{2+} ions moving into the crack react with dissolved CO_2, $CaCO_3$ is generated. Thus, $CaCO_3$ generated usually has very low solubility (insoluble property) and fills the cracks. As the second stage has a much lower crack self-healing performance than the further hydration of the first stage, crack healing occurs quickly at early age and is mitigated later.

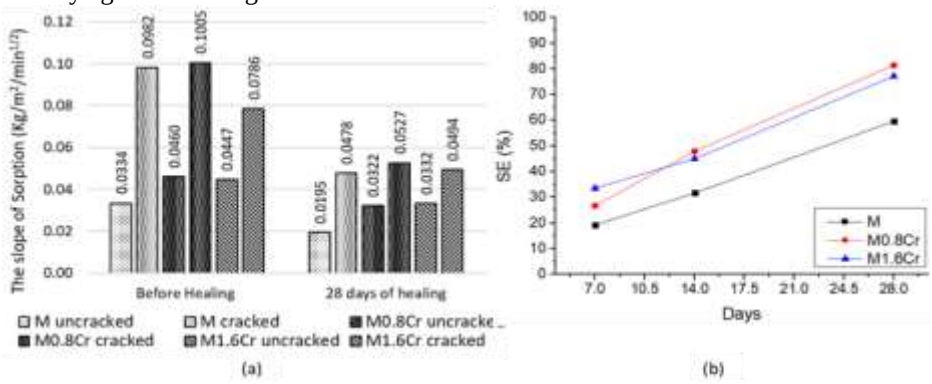

Fig. 4. (a) The slope of sorption before and after the healing period of 28 days, (b) and the Sealing Efficiency of all the compositions, after 7, 14, and 28 days

To exclude the microstructure factor, the healing efficiency was calculated based on equation 1. Figure 4(b) depicts the SE of the compositions' SE after 7, 14, and 28 days of healing. According to that, at all ages, the healing rate was higher than the plain composition. Specifically, at 7 days, the SE of M, M0.8Cr, and M1.6Cr was 19%, 27%, and 34%, respectively. The increased crystalline content seems to accelerate the initial reaction to the surface, especially with 1.6%. Subsequently, at 14 and 28 days, the SE seems to have the same trend presenting even greater SE. Finally, after 28 days, the SE of M, M0.8Cr, and M1.6Cr was 60%, 81%, and 77%, respectively.

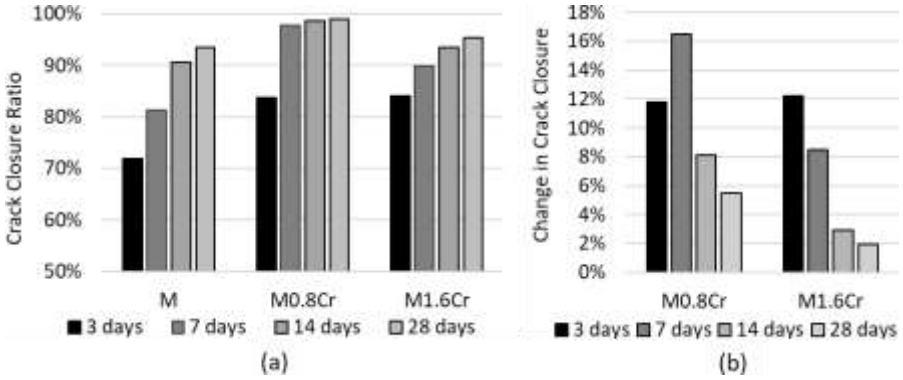

Fig. 5. (a) Crack closure of all compositions, and (b) Change in the Crack closure comperared to the reference sample, after 3, 7, 14, and 28 days.

Similar to SE, the crack closure ratio (CCR) has been calculated based on equation 2. Figure 5 depicts the CCR of all compositions after 3, 7, 14, and 28 days of healing. According to that, the composition with CAs seems to improve the crack's surface

healing after 3 and 7 days of hydration. After 14 days of healing, the CCR was above 90% for all compositions, with M0.8Cr exhibit the most remarkable results, reaching almost 100% of healing after 28 days. The results are in line with the SE results, proving that even the mere counting of the surface crack undermines the healing ability and that the crystallites favored healing.

3.3 Recovery of compressive strength

Figure 6 shows the healing rate of the pre-damaged cubes after one month of healing. The recovery of compressive strength, according to equation 3 evaluated based on the level of damage caused in each sample. The level of damage has been estimated based on the ultrasonic pulse velocity before and after the pre-damage. According to fig. 6(a). the level of damage was similar for reference and M1.6Cr, with an average damage of 26.1% and 27.1%, respectively. Although in the case of M0.8Cr, the level of damage rises to 38.5%. The fig. 6(b) shows that the RCS of the reference sample was 76% of the initial compressive strength. On the other hand, the recovery index of compositions with CA was 92.5%, 92.9% for M0.8Cr, and M1.6Cr, respectively. Those rates prove the very important contribution of the CAs that superficially close the crack and increase their strength. This increase was due to the ability to heal the cracks inside the structure and increase the strength of the healing agents.

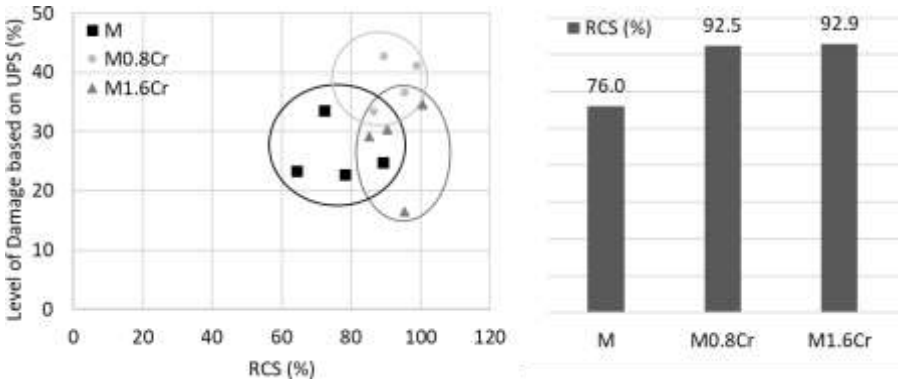

Fig. 6. The Recovery of Compressive Strength (RCS) to the level of damage based on UPS (%), (b) The average RCS(%) of all compositions after one month of healing.

3.4 3D acoustic Tomography

The M0.8Cr composition was measured via the acoustic microscopy setup, an unhealed specimen with visible cracking, and its healed counterpart. The tomographic image of the former, depicted in Fig. 7(a), clearly indicates the propagation of the cracking through. Moreover, a C-scan image is evaluated in Fig. 7(c) for this sample at 2 mm depth from the concrete surface, revealing the inner cracking profile. Finally, the tomographic image of the healed counterpart is illustrated in Fig. 7(b), proving the almost perfect healing due to a cracking absence.

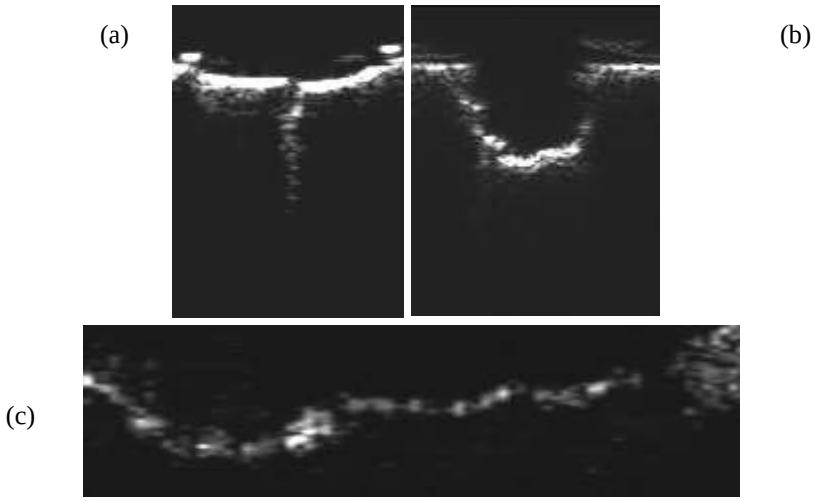

Fig. 7. Tomographic images, ac-quired via a 75 MHz acoustic microscope of (a) a concrete sample with cracking and (b) its healed counterpart. (c) The cracking profile of the first concrete sample at 2 mm depth.

4 Conclusions

This study investigates the self-healing performance and physic-mechanical properties of artificial stone. The effect of CAs on the mechanical properties was evident, as the compressive strength and the modulus of elasticity reduced, indicating the impact on the microstructure of the composition. Although the ability of CAs to heal and feel the gaps was profound to the flexural analysis, achieving a 50% strength rise in both compositions. Additionally, the porosity and capillary test have been significantly reduced at early-age for compositions with CAs. While the hydrophilic nature of the CAs prevents the same rate from continuing after 28 days.

For the self-healing evaluation, the pre-cracking samples on the sorption had a greater correlation with the level of damage than the initial crack width. This fact showed that even the crack had been isolated, the microstructure still plays a crucial role. Despite this fact, the healing rate of the composition with CAs has increased approximately by 20%. Additionally, the recovery of the compressive strength of cubes that have been pre-damaged to failure proved that the CAs react in the surface and also in the 'diffusion control' stage. In this stage, healing occurs inside the cracks, and healing agents with increased strength have been created, leading to 20% increased recovery. The composition with better healing efficiency, M0.8Cr, was analysed through 3D acoustic tomography. The outcome of this test showed that it was not possible to detect the crack with the resolution of 20μm. This fact proved that the healing had been achieved to such an extent that it will not be able to detect.

The results of the healing efficiency were quite interesting and constant. The CAs have established their beneficial role. The increased CAs seemed to play a minor role

in the healing properties, proving that 0.8% was the ideal portion.

Acknowledgments

Author Tsampali E. would like to thank the General Secretariat for Research and Technology (GSRT) and the Hellenic Foundation for Research and Innovation (HFRI) for funding the research through the scholarship funding program for Ph.D. candidate

References

1. Papayianni I. Design of compatible repair materials for the restoration of monuments. Int J Restor 2004;1–6:623–36.
2. Gooch JW. Encyclopedic dictionary of polymers. Atlanda: Springer; 2011.
3. M. Stefanidou, V. Pachta, I. Papayianni Design and testing of artificial stone for the resto- ration of stone elements in monuments and historic buildings Construction and Building Materials Volume 93, 15 September 2015, Pages 957-965
4. Lee MY, Ko CH, Chang FC, Lo SL, Lin JD, Shan MY, et al. Artificial stone slab production using waste glass, stone fragments and vacuum vibratory compaction. Cement Concr Compos 2008;30:583–7.
5. C. Edvardsen, Water permeability and autogenous healing of cracks in concrete, ACI Mater. J. 96 (4) (1999) 448–454.
6. M. Roig-Flores, F. Pirritano, P. Serna, L. Ferrara, Effect of crystalline admixtures on the self-healing capability of early-age concrete studied by means of permeability and crack closing tests, Construction and Building Materials 114 (2016) 447–457
7. M. Stefanidou, E. Evangelia, et. al., Techniques for recording self-healing efficiency and characterizing the healing products in cementitious materials, Material Design & Processing Communication, Volume 3, Issue 3, (2020)
8. E. Tsampali, E. Yfantidis, A. Ioakim, M. Stefanidou, Efficacy of different crystalline admixtures in self-healing capacity of fibre reinforced concrete, Lorcenis Conference (2019).
9. Briggs, Andrew, ed. Advances in acoustic microscopy. Vol. 1. Springer Science & Business Media, 2013.